PAPER

Temperature-dependent photoluminescence emission and Raman scattering from $Mo_{1-x}W_xS_2$ monolayers

To cite this article: Yanfeng Chen *et al* 2016 *Nanotechnology* **27** 445705

IOP Publishing Nanotechnology
Nanotechnology 27 (2016) 445705 (6pp) doi:10.1088/0957-4484/27/44/445705

Temperature-dependent photoluminescence emission and Raman scattering from $Mo_{1-x}W_xS_2$ monolayers

Yanfeng Chen[1,6], Wen Wen[1,2,6], Yiming Zhu[1], Nannan Mao[1,3], Qingliang Feng[1], Mei Zhang[1,2], Hung-Pin Hsu[4], Jin Zhang[3], Ying-Sheng Huang[5] and Liming Xie[1,2]

[1] CAS Key Laboratory of Standardization and Measurement for Nanotechnology, CAS Center for Excellence in Nanoscience, National Center for Nanoscience and Technology, Beijing 100190, People's Republic of China
[2] University of Chinese Academy of Sciences, Beijing 100049, People's Republic of China
[3] Center for Nanochemistry, College of Chemistry and Molecular Engineering, Peking University, Beijing 100871, People's Republic of China
[4] Department of Electronic Engineering, Ming Chi University of Technology, Taipei 106, Taiwan, Republic of China
[5] Department of Electronic Engineering, National Taiwan University of Science and Technology, Taipei 106, Taiwan, Republic of China

E-mail: xielm@nanoctr.cn

Received 14 April 2016, revised 9 August 2016
Accepted for publication 22 August 2016
Published 27 September 2016

Abstract

2D transition metal dichalcogenide (TMD) alloys with tunable band gaps have recently gained wide interest due to their potential applications in future nanoelectronics and optoelectronics. Here, we report the temperature-dependent photoluminescence (PL) and Raman spectra of $Mo_{1-x}W_xS_2$ monolayers with W composition $x = 0$, 0.29, 0.53, 0.66 and 1 in the temperature range 93–493 K. We observed a linear temperature dependence of PL emission energy and Raman frequency. The PL intensity is enhanced at high temperature (>393 K). The temperature coefficients are negative for both PL and Raman bands, which may result from anharmonicity, thermal expansion and composition disorder.

Keywords: transition metal dichalcogenide, 2D material, alloy, Raman spectroscopy, photoluminescence, temperature dependence

Introduction

2D atomic crystal, such as graphene [1–6], BN [7], and transition metal dichalcogenides (TMDs) MX_2 (M=Mo, W, Nb, Ta; X=S, Se, Te) [8–21] have attracted wide interest in recent years due to their unique structures, special physical properties and potential applications. Group VIB TMDs, such as MoX_2 and WX_2 (X=S, Se) are especially interesting for electronic and optoelectronic applications [11, 22–24] because of their nonzero direct band gap [10, 25] and the emergence of strong photoluminescence (PL) in single-layer form [12, 16, 17]. Band gap engineering of 2D materials is of importance for promising nano-optoelectronics [3, 26–29]. Alloying different TMDs to achieve a tunable band gap in 2D monolayers has recently been proposed by theoretical calculations [30, 31] and demonstrated by experiments [32–38]. Knowledge of a material's thermal properties is critical, because heat dissipation is one of the most significant constraints in the design and fabrication of integrated electronic circuits [5, 6]. Micro-Raman/PL spectroscopy is a non-invasive yet powerful technique to characterize the structures and thermal properties of 2D materials [5]. Here, we present a study of the temperature dependence of PL and Raman spectra of $Mo_{1-x}W_xS_2$ monolayer alloys ($x = 0$, 0.29, 0.53,

[6] These authors contributed equally to this work.

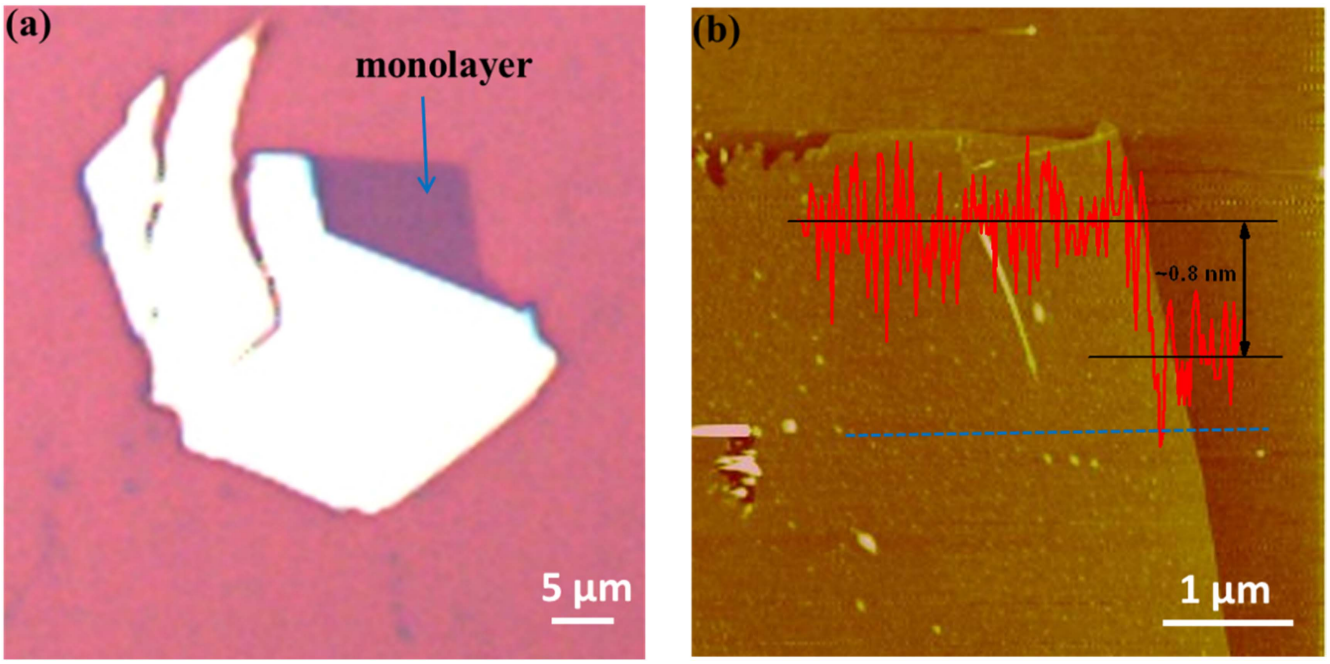

Figure 1. (a) Optical and (b) AFM images of a $Mo_{0.47}W_{0.53}S_2$ monolayer.

0.66 and 1) in the temperature range 93–493 K. Both PL emission and the first-order Raman modes redshift with increasing temperature. The PL intensity first decreases and then increases with temperature increase.

Experiment section

Sample preparation

$Mo_{1-x}W_xS_2$ single crystals were grown by the chemical vapor transport method [39, 40] using $Mo_{1-x}W_xS_2$ powders (synthesized from Mo, W and S powders) with Br_2 as the transport agent at 1030 °C–980 °C. 2H-type layered structures and alloy compositions for all $Mo_{1-x}W_xS_2$ crystals were confirmed by x-ray diffraction (XRD) and energy dispersive x-ray spectroscopy (EDX), respectively, which was reported previously [39]. $Mo_{1-x}W_xS_2$ monolayer samples were mechanically exfoliated from bulk $Mo_{1-x}W_xS_2$ single crystals using a similar technique employed for graphene [1] and transferred to the Si/SiO_2 (300 nm SiO_2) substrates.

Characterization

The location, shape and layer number of the $Mo_{1-x}W_xS_2$ flakes were identified by a combination of optical contrast in an optical microscope image and atomic force microscopy (AFM) imaging, as shown in our previous work [33].

PL and Raman measurements were performed on a JY Horiba HR800 micro-Raman/PL system. All spectra were excited with 514.5 nm laser light and collected in a back-scattering configuration. We used a 50x objective to focus the excitation laser on the $Mo_{1-x}W_xS_2$ monolayer alloys. The sample temperature was controlled by a cold-hot cell operated using a liquid nitrogen source (Linkam THMS600). All measurements were carried out under ambient conditions at low excitation power. The power on top of the cold-hot cell quartz window was below 3 mW. The accuracy of the cell temperature control was ±1 K.

Results and discussion

The $Mo_{1-x}W_xS_2$ monolayer flakes were cleaved from the corresponding bulk single crystals onto SiO_2/Si substrates (oxide thickness of 300 nm). Optical imaging and AFM imaging (figures 1(a) and (b)) were used to locate and identify the $Mo_{1-x}W_xS_2$ monolayers, as reported in our previous work [33].

Figure 2(a) shows a schematic of the experimental setup. Temperature-dependent PL spectra of the $Mo_{1-x}W_xS_2$ monolayer alloys with different W composition x (0, 0.29, 0.53, 0.66 and 1) in the range 93–493 K are shown in figures 2(b)–(f). For $Mo_{1-x}W_xS_2$ monolayer alloys with $x = 0$, 0.29, 0.53 and 0.66, the PL spectra show one strong PL peak, i.e. A-exciton emission (low-energy one), with a weak shoulder B-exciton emission peak at the higher energy side. The splitting of A-, B-excitons are due to valance band spin–orbit coupling [12]. The PL spectra of the WS_2 monolayer show only one A-exciton emission peak. The PL peaks were fitted by Gaussian functions. The temperature-dependent PL peak intensities and positional shifts are plotted in figures 3(a)–(c), respectively. For all $Mo_{1-x}W_xS_2$ monolayers, A-exciton emission intensity first decreases and then increases with increasing temperature. Generally, temperature-dependent PL intensity can be

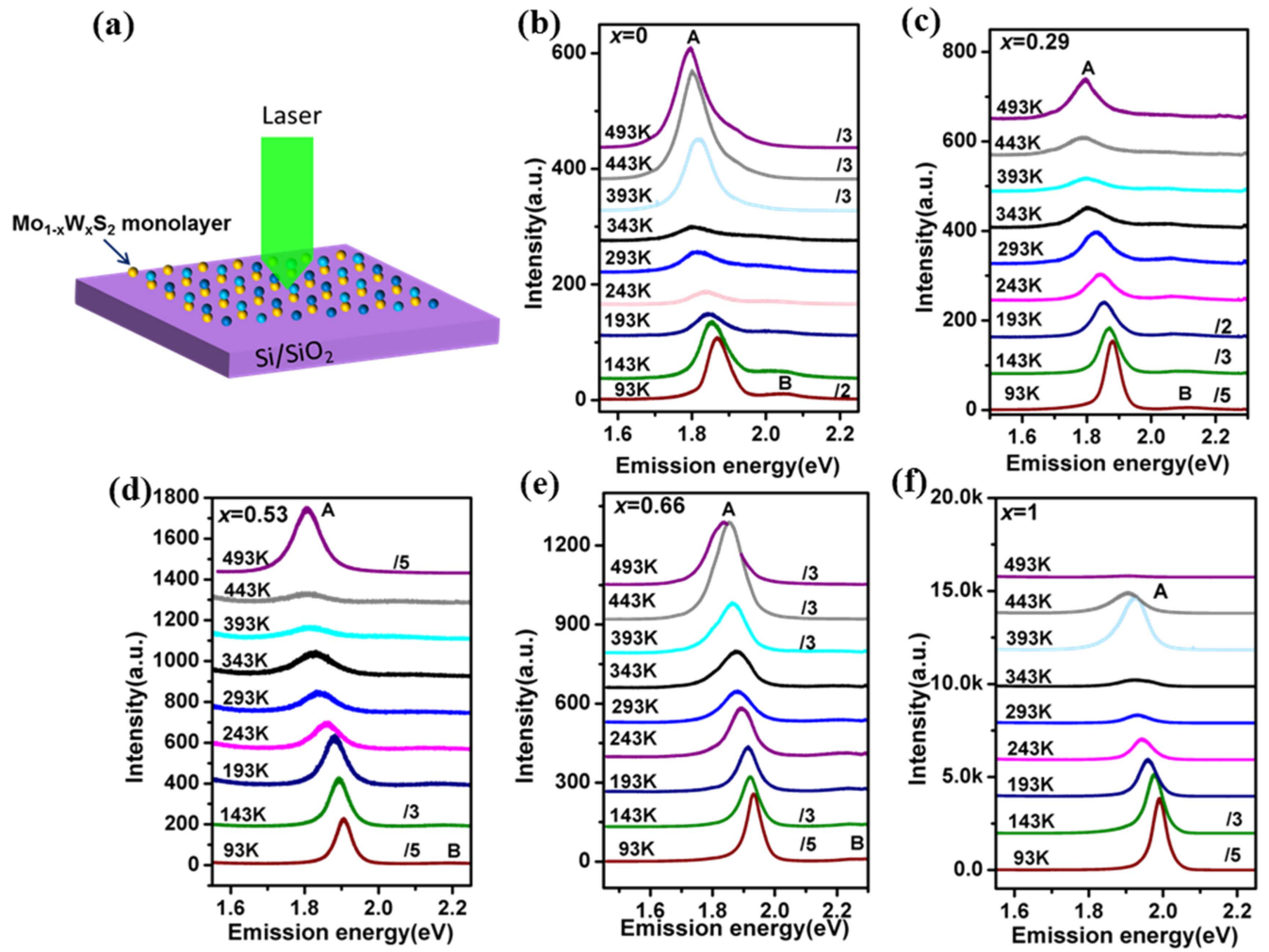

Figure 2. Schematic of the experimental setup (a) and temperature-dependent (93–493 K) PL spectra of the $Mo_{1-x}W_xS_2$ monolayer alloys with different W composition x, (b) $x = 0$, (c) $x = 0.29$, (d) $x = 0.53$, (e) $x = 0.66$, (f) $x = 1$.

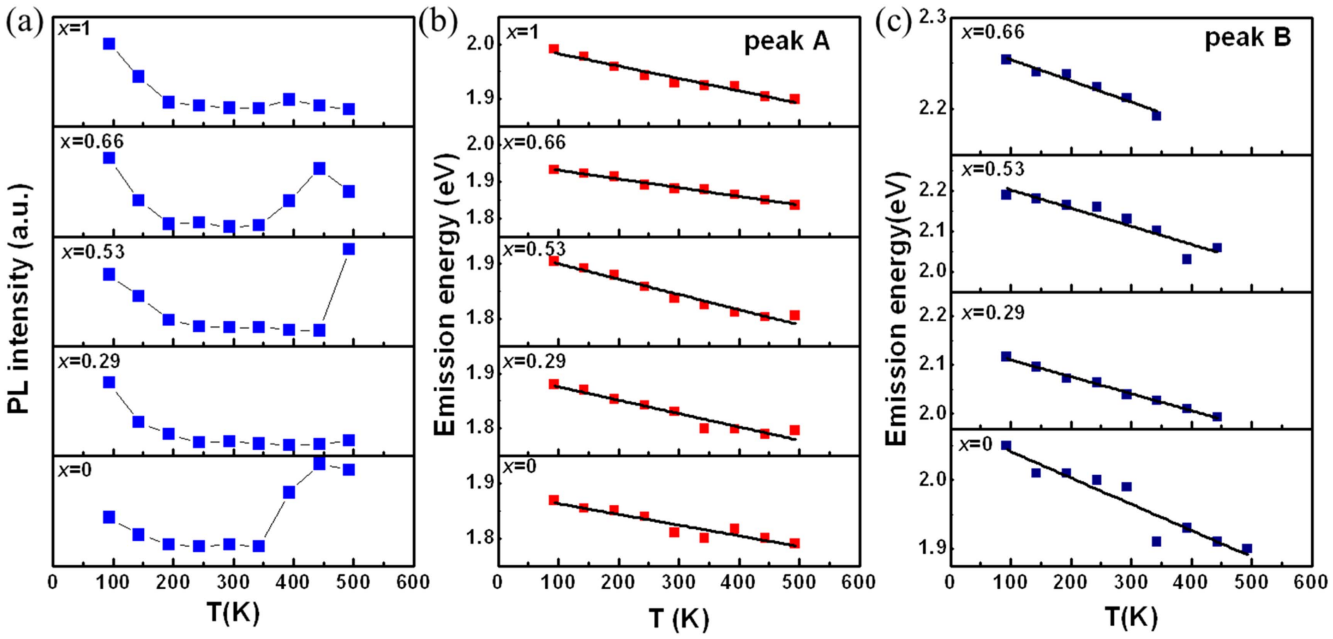

Figure 3. Temperature-dependent emission intensity of A-exciton (a) and peak positions for (b) A-exciton and (c) B-exciton of the $Mo_{1-x}W_xS_2$ monolayers with different W composition x. The black lines show the fitting results using equation (2).

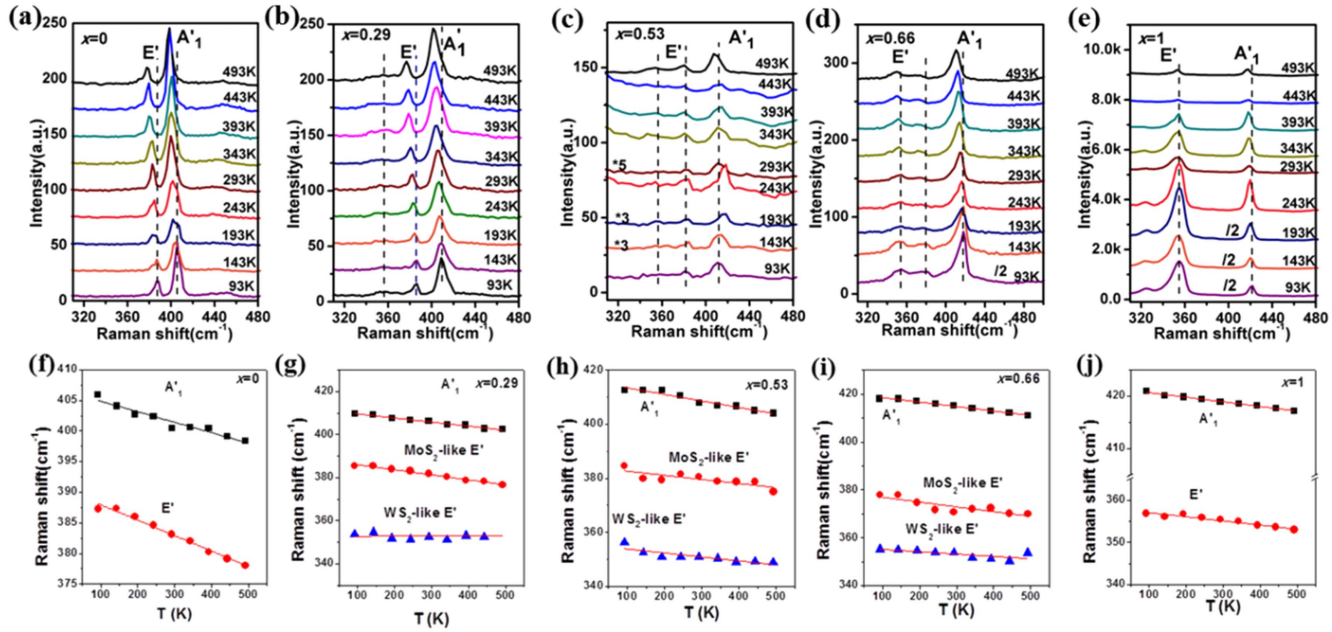

Figure 4. Temperature-dependent Raman spectra (a)–(e) and the peak positions of the first-order Raman modes A_1', MoS_2-like and WS_2-like E'(f)–(j) in the $Mo_{1-x}W_xS_2$ monolayer alloys with different W composition x (0, 0.29, 0.53, 0.66, 1). The dashed lines in panel (a)-(e) are a visual guide. The lines in panel (f)-(j) show the fitting results using equation (3).

Table 1. Fitted temperature coefficients for PL emission energies for the $Mo_{1-x}W_xS_2$ monolayers.

x	0	0.29	0.53	0.66	1
α_A (meV K^{-1})	−0.20	−0.24	−0.28	−0.24	−0.23
α_B (meV K^{-1})	−0.38	−0.35	−0.45	−0.23	/

expressed by [41]

$$I_{PL}(T) = I_0 \times k_r(T)/(k_r(T) + k_{nr}(T)) \quad (1)$$

where I_0 is the maximum PL intensity as T approaches 0 K, and $k_r(T)$ and $k_{nr}(T)$ are the temperature-dependent radiative and nonradiative recombination rates, respectively. The nonradiative recombination rates $k_{nr}(T)$ can be from the defect trapping rates k_{defect} and electron relaxation within the conduction and valance band k_{relax} [12]. The general trend is that the PL intensity as well as quantum efficiency dramatically decrease as the temperature increases, which is attributed to the thermally activated nonradiative recombination due to the increased electron–phonon interactions.

At high temperature range (>393 K), the PL intensity is dramatically enhanced by more than 20 times. This may be due to defect generation after higher temperatures in which the defect sites have higher emission efficiency [41]. The as-exfoliated MoS_2 monolayer is normally n-doped, due to the presence of defects or unintentional substrate doping [13]. We can deduce that there are two different mechanisms that simultaneously influence the PL intensity, i.e. radiative recombination rates and physical/chemical doping. The low PL intensity for trions at mediate temperature could be connected with faster nonradiative decays [41].

The temperature-dependent emission energy was plotted in figures 3(b) and (c). Both A- and B-exciton emission energies redshift as the temperature increases for all the $Mo_{1-x}W_xS_2$ monolayers. The observed decrease in the optical band gap as a function of temperature is similar to that observed in semiconductors, which is due to increased electron–phonon interactions as well as lattice expansion at high temperatures [42, 43]. The temperature dependence of the band gap in semiconductors is usually fitted by the empirical Varshni relation [42], $E_g = E_0 - (\alpha T^2)/(T + \beta)$, where the parameters α and β are constants. Here, a simpler analytical expression is used to fit the temperature dependence of the energy band gap in the $Mo_{1-x}W_xS_2$ monolayer alloys [44],

$$E_g(T) = E_g(0) + \alpha T \quad (2)$$

where $E_g(0)$ is the band gap value as T approaches 0 K, α is the temperature coefficient of $E_g(T)$. A negative α value was observed for the $Mo_{1-x}W_xS_2$ monolayer (table 1). For A-exciton, as W composition changes, α value ranges from −0.20 to −0.28 meV K^{-1}. For B-exciton, α value ranges from −0.23 to −0.45 meV K^{-1}. The α value reaches its maximum value at the intermediate composition alloy, i.e. the $Mo_{0.47}W_{0.53}S_2$ monolayer.

Figure 4 shows temperature-dependent Raman spectra (figures 4(a)–(e)) and frequencies (figures 4(f)–(j)) of the $Mo_{1-x}W_xS_2$ monolayers. For the MoS_2 monolayer, there is strong Raman scattering for both E' and A_1' modes at all temperatures. For the WS_2 monolayer, the Raman intensities of 2LA(M) + E' and A_1' modes become very weak at high temperatures (443 and 493 K) (figure 4(e)). The decrease in Raman intensities at 443 and 493 K may be due to the oxidization and/or defect generation of the WS_2 monolayer.

Table 2. Temperature coefficients of the first-order Raman modes A_1', MoS_2-like and WS_2-like E′ for the $Mo_{1-x}W_xS_2$ monolayers.

x	0	0.29	0.53	0.66	1
$\chi_{A_1'}(cm^{-1}\,K^{-1})$	−0.017	−0.019	−0.024	−0.019	−0.009
χMoS_2-like E' $(cm^{-1}\,K^{-1})$	−0.025	−0.024	−0.015	−0.020	/
χWS_2-like $E'(cm^{-1}\,K^{-1})$	/	−0.004	−0.015	−0.01	−0.01

All first-order Raman active modes A_1', MoS_2-like E' and WS_2-like E' redshift as the temperature increases (figures 4(f)–(j)). The observed temperature-dependent peak positions can be fitted using the Grüneisen model [45–47]

$$\omega(T) = \omega_0 + \chi T \tag{3}$$

where ω_0 is the frequency as T approaches 0 K and χ is the first-order temperature coefficient of the Raman modes. Negative χ values for A_1' and E' modes in the $Mo_{1-x}W_xS_2$ monolayers have been obtained (table 2). The temperature-dependent Raman shift is attributed to the anharmonic contributions to the interatomic potential energy, mediated by phonon–phonon interaction [42, 48].

For the MoS_2 monolayer, the temperature coefficients of A_1' and E' modes are -0.017 and $-0.025\,cm^{-1}\,K^{-1}$, respectively, which are close to those of the sapphire supported MoS_2 monolayer ($-0.013\,cm^{-1}\,K^{-1}$ for A_1' and $-0.017\,cm^{-1}\,K^{-1}$ for E') and chemical vapor deposition (CVD) grown MoS_2 monolayer ($-0.016\,cm^{-1}\,K^{-1}$ for A_1' and $-0.013\,cm^{-1}\,K^{-1}$ for E') [49, 50]. For the WS_2 monolayer, the temperature coefficients of A_1' and E' modes are -0.009 and $-0.010\,cm^{-1}\,K^{-1}$, respectively, which are close to those of previously reported single-layer WS_2 ($-0.006\,cm^{-1}\,K^{-1}$ for both A_1' and E') [51]. For the $Mo_{1-x}W_xS_2$ monolayer with $x = 0.29$, 0.53 and 0.66, the temperature coefficients of the first-order Raman modes A_1' and WS_2-like E' reach their maximum at $x = 0.53$ (table 2), which is similar to the trend of temperature coefficient change of A emission energy. While for the MoS_2-like E' mode, the temperature coefficient reaches its minimum at $x = 0.53$.

Conclusions

We have systematically measured the temperature-dependent PL and Raman spectra of the $Mo_{1-x}W_xS_2$ monolayer with $x = 0$, 0.29, 0.53, 0.66 and 1. We observed that the PL intensities of the $Mo_{1-x}W_xS_2$ monolayer alloys first decrease (due to electron–phonon interaction) and then increase with temperature increasing. The unexpected increase in PL intensity at high temperature may be attributed to defect generation at higher temperatures. The PL and Raman peaks redshift as temperature increases in the temperature range 93 −493 K, which is attributed to the anharmonic effects and composition disorder.

Acknowledgments

The authors acknowledge support from the National Natural Science Foundation of China (NNSFC) (21373066 and 11304052), the Beijing Nova Programme (Z151100000315081), the Beijing Talents Fund (2015000021223ZK17), the China Postdoctoral Science Foundation (2013M540900) and the support of the Ministry of Science and Technology of Taiwan under Project nos. MOST104-2112-M-011-003 and MOST104-2221-E-131-001-MY2.

References

[1] Novoselov K, Geim A K, Morozov S, Jiang D, Zhang Y, Dubonos S, Grigorieva I and Firsov A 2004 Electric field effect in atomically thin carbon films *Science* **306** 666–9
[2] Xia F, Mueller T, Lin Y-M, Valdes-Garcia A and Avouris P 2009 Ultrafast graphene photodetector *Nat. Nanotechol.* **4** 839–43
[3] Balog R *et al* 2010 Bandgap opening in graphene induced by patterned hydrogen adsorption *Nat. Mater.* **9** 315–9
[4] Xia F, Farmer D B, Lin Y-M and Avouris P 2010 Graphene field-effect transistors with high on/off current ratio and large transport band gap at room temperature *Nano Lett.* **10** 715–8
[5] Ghosh S, Bao W, Nika D L, Subrina S, Pokatilov E P, Lau C N and Balandin A A 2010 Dimensional crossover of thermal transport in few-layer graphene *Nat. Mater.* **9** 555–8
[6] Ghosh S, Calizo I, Teweldebrhan D, Pokatilov E P, Nika D L, Balandin 1 B-W, Bao A A, Miao F and Lau C N 2008 Extremely high thermal conductivity of graphene: Prospects for thermal management applications in nanoelectronic circuits *Appl. Phys. Lett.* **92** 151911
[7] Lin Y and Connell J W 2012 Advances in 2D boron nitride nanostructures: nanosheets, nanoribbons, nanomeshes, and hybrids with graphene *Nanoscale* **4** 6908–39
[8] Chhowalla M, Shin H S, Eda G, Li L-J, Loh K P and Zhang H 2013 The chemistry of two-dimensional layered transition metal dichalcogenide nanosheets *Nat. Chem.* **5** 263–75
[9] Lee C, Yan H, Brus L E, Heinz T F, Hone J and Ryu S 2010 Anomalous lattice vibrations of single-and few-layer MoS_2 *ACS Nano* **4** 2695–700
[10] Mak K F, Lee C, Hone J, Shan J and Heinz T F 2010 Atomically thin MoS_2: a new direct-gap semiconductor *Phys. Rev. Lett.* **105** 136805
[11] Wang Q H, Kalantar-Zadeh K, Kis A, Coleman J N and Strano M S 2012 Electronics and optoelectronics of two-dimensional transition metal dichalcogenides *Nat. Nanotechnol.* **7** 699–712
[12] Splendiani A, Sun L, Zhang Y, Li T, Kim J, Chim C-Y, Galli G and Wang F 2010 Emerging photoluminescence in monolayer MoS_2 *Nano Lett.* **10** 1271–5

[13] Tongay S *et al* 2013 Broad-range modulation of light emission in two-dimensional semiconductors by molecular physisorption gating *Nano Lett.* **13** 2831–6

[14] Ye G, Gong Y, Lin J, Li B, He Y, Pantelides S T, Zhou W, Vajtai R and Ajayan P M 2016 Defects engineered monolayer MoS_2 for improved hydrogen evolution reaction *Nano Lett.* **16** 1097–103

[15] Su W, Dou H, Huo D, Dai N and Yang L 2015 Enhancing photoluminescence of trion in single-layer MoS_2 using p-type aromatic molecules *Chem. Phys. Lett.* **635** 40–4

[16] Gutiérrez H R *et al* 2013 Extraordinary room-temperature photoluminescence in triangular WS_2 monolayers *Nano Lett.* **13** 3447–54

[17] Li H, Zhang Q, Yap C C R, Tay B K, Edwin T H T, Olivier A and Baillargeat D 2012 From bulk to monolayer MoS_2: evolution of Raman scattering *Adv. Funct. Mater.* **22** 1385–90

[18] Heinz T F *et al* 2013 Progress, challenges, and opportunities in two-dimensional materials beyond graphene *ACS Nano* **7** 2898–926

[19] Tonndorf P *et al* 2013 Photoluminescence emission and Raman response of monolayer MoS_2, $MoSe_2$, and WSe_2 *Opt. Express* **21** 4908–16

[20] Zhang X, Qiao X-F, Shi W, Wu J-B, De-Sheng Jiang D-S and Tan P-H 2015 Phonon and Raman scattering of two-dimensional transition metal dichalcogenides from monolayer, multilayer to bulk material *Chem. Soc. Rev.* **44** 2757–85

[21] Qiao X-F, Li X-L, Zhang X, Shi W, Wu J-B, Chen T and Tan P-H 2015 Substrate-free layer-number identification of two-dimensional materials: A case of $Mo_{0.5}W_{0.5}S_2$ alloy *Appl. Phys. Lett* **106** 223102

[22] Kim S *et al* 2012 High-mobility and low-power thin-film transistors based on multilayer MoS_2 crystals *Nat. Commun.* **3** 1011–7

[23] Yoon Y, Ganapathi K and Salahuddin S 2011 How good can monolayer MoS_2 transistors be? *Nano Lett.* **11** 3768–73

[24] Lee H S, Min S-W, Chang Y-G, Park M K, Nam T, Kim H, Kim J H, Ryu S and Im S 2012 MoS_2 nanosheet phototransistors with thickness-modulated optical energy gap *Nano Lett.* **12** 3695–700

[25] Kuc A, Zibouche N and Heine T 2011 Influence of quantum confinement on the electronic structure of the transition metal sulfide TS_2 *Phys. Rev.* B **83** 245213

[26] Xie L, Wang H, Jin C, Wang X, Jiao L, Suenaga K and Dai H 2011 Graphene nanoribbons from unzipped carbon nanotubes: atomic structures, Raman spectroscopy, and electrical properties *J. Am. Chem. Soc.* **133** 10394–7

[27] Yue Q, Chang S, Kang J, Zhang X, Shao Z, Qin S and Li J 2012 Bandgap tuning in armchair MoS_2 nanoribbon *J. Phys. Condens. Matter* **24** 335501

[28] Zhang Y, Tang T-T, Girit C, Hao Z, Martin M C, Zettl A, Crommie M F, Shen Y R and Wang F 2009 Direct observation of a widely tunable bandgap in bilayer graphene *Nature* **459** 820–3

[29] Zanella I, Guerini S, Fagan S, Mendes Filho J and Souza Filho A 2008 Chemical doping-induced gap opening and spin polarization in graphene *Phys. Rev.* B **77** 073404

[30] Komsa H-P and Krasheninnikov A V 2012 Two-dimensional transition metal dichalcogenide alloys: Stability and electronic properties *J. Phys. Chem. Lett.* **3** 3652–6

[31] Kang J, Tongay S, Li J and Wu J 2013 Monolayer semiconducting transition metal dichalcogenide alloys: stability and band bowing *J. Appl. Phys.* **113** 143703–7

[32] Zhang M *et al* 2014 Two-dimensional molybdenum tungsten diselenide alloys: photoluminescence, Raman scattering, and electrical transport *ACS Nano* **8** 7130–7

[33] Chen Y, Xi J, Dumcenco D O, Liu Z, Suenaga K, Wang D, Shuai Z, Huang Y-S and Xie L 2013 Tunable band-gap photoluminescence from atomically thin transition-metal dichalcogenide alloys *ACS Nano* **7** 4610–6

[34] Feng Q *et al* 2014 Growth of large-area 2D $MoS2_{(1-x)}Se_{2x}$ semiconductor alloys *Adv. Mater.* **26** 2648–53

[35] Li H *et al* 2014 Growth of alloy $MoS_{2x}Se_{2(1-x)}$ nanosheets with fully tunable chemical compositions and optical properties *J. Am. Chem. Soc.* **136** 3756–9

[36] Mann J *et al* 2014 2-dimensional transition metal dichalcogenides with tunable direct band gaps: $MoS_{2(1-x)}Se_{2x}$ monolayers *Adv. Mater.* **26** 1399–404

[37] Li H *et al* 2015 Lateral growth of composition graded atomic layer $MoS_{2(1-x)}Se_{2x}$ nanosheets *J. Am. Chem. Soc.* **137** 5284–7

[38] Feng Q, Mao N, Wu J, Xu H, Wang C, Zhang J and Xie L 2015 Growth of $MoS_{2(1-x)}$ Se_{2x} ($x = 0.41$–1.00) monolayer alloys with controlled morphology by physical vapor deposition *ACS Nano* **9** 7450–5

[39] Dumcenco D, Chen K, Wang Y, Huang Y and Tiong K 2010 Raman study of 2H-Mo_{1-x} W_xS_2 layered mixed crystals *J. Alloys Compd.* **506** 940–3

[40] Dumcenco D O, Su Y-C, Wang Y-P, Chen K-Y, Huang Y-S, Ho C-H and Tiong K-K 2011 Polarization dependent Raman active modes study of the $Mo_{1-x}W_xS_2$ mixed layered crystals *Chin. J. Phys.* **49** 270–7

[41] Nan H *et al* 2014 Strong photoluminescence enhancement of MoS_2 through defect engineering and oxygen bonding *ACS Nano* **8** 5738–45

[42] Varshni Y P 1967 Temperature dependence of the energy gap in semiconductors *Physica* **34** 149–54

[43] O'Donnell K and Chen X 1991 Temperature dependence of semiconductor band gaps *Appl. Phys. Lett.* **58** 2924–6

[44] Bludau W, Onton A and Heinke W 1974 Temperature dependence of the band gap of silicon *J. Appl. Phys.* **45** 1846–8

[45] Calizo I, Balandin A, Bao W, Miao F and Lau C 2007 Temperature dependence of the Raman spectra of graphene and graphene multilayers *Nano Lett.* **7** 2645–9

[46] Yoon D, Son Y-W and Cheong H 2011 Negative thermal expansion coefficient of graphene measured by Raman spectroscopy *Nano Lett.* **11** 3227–31

[47] Tan P-H, Deng Y-M, Zhao Q and Cheng W-C 1999 The intrinsic temperature effect of the Raman spectra of graphite *Appl. Phys. Lett.* **74** 1818–20

[48] Tongay S, Zhou J, Ataca C, Lo K, Matthews T S, Li J, Grossman J C and Wu J 2012 Thermally driven crossover from indirect toward direct bandgap in 2D semiconductors: $MoSe_2$ versus MoS_2 *Nano Lett.* **12** 5576–80

[49] Lanzillo N A *et al* 2013 Temperature-dependent phonon shifts in monolayer MoS_2 *Appl. Phys. Lett.* **103** 093102

[50] Yan R *et al* 2014 Thermal conductivity of monolayer molybdenum disulfide obtained from temperature-dependent Raman spectroscopy *ACS Nano* **8** 986–93

[51] Nagaleekar T and Late D J 2014 Temperature dependent phonon shifts in single-layer WS_2 *ACS Appl. Mater. & Inter.* **6** 1158–63